Journal of the Mechanical Behavior of Biomedical Materials 171 (2025) 107135

Contents lists available at ScienceDirect

Journal of the Mechanical Behavior of Biomedical Materials

journal homepage: www.elsevier.com/locate/jmbbm

Bio-inspired design and finite element analysis of polymer composite microneedles with hollow architecture

Md Rahatuzzaman, Erina Baynojir Joyee *

Department of Mechanical Engineering and Engineering Science, University of North Carolina at Charlotte, Charlotte, NC, 28223, USA

ARTICLE INFO

Keywords:
Hollow microneedle
Interstitial fluid
FEA
Silicon carbide
Multimaterial μDLP

ABSTRACT

Interstitial fluid (ISF) is a body fluid found in dermal cells containing different types of biomarkers. Microneedles have been developed for transdermal applications such as drug delivery and the extraction of dermal fluids. In this study, a micro digital light processing (μDLP) technique is utilized to fabricate a fountain pen inspired hollow microneedle (HMN) patch. This research focused on evaluating the optimal design parameters and print angle of HMN with high resolution. Furthermore, ANSYS finite element analysis (FEA) evaluated that the maximum von-Mises stress of individual needle tip is 3.291 MPa which is greater than the skin resistance value of 3.183 MPa. Simple stress, such as tensile or compressive stress, measures force per unit area applied in one direction. In contrast, von-Mises stress combines stresses from multiple directions. This approach provides a more accurate prediction of failure in microneedles under complex loading conditions. In addition to that, the maximum total deformation is 6.1034 μm which is smaller than the length of the microneedle. Moreover, Silicon Carbide (SiC) is introduced as filler ceramic material to fabricate the hollow microneedle patch.

1. Introduction

Interstitial fluid (ISF) is a peripheral fluid that is a rich source of physiological information (Kool et al., 2007). It can serve as a source of biomarkers for diagnosing various chronic conditions, including diabetes and hyperlipidemia (Kolluru et al., 2019; Teymourian et al., 2020). In order to sample these biomarkers, hollow microneedle (HMN) patches were developed as an extraction device in recent years (Wang et al., 2021). Traditional methods, such as suction blister (Kiistala, 1968), microdialysis (Bajramaj et al., 2019), and sonophoresis (Kost et al., 2000), were used to extract ISF before the microneedling technique. Suction blister technique is a time consuming, invasive, and discomforting technique to extract the ISF which results in patient discomfort and damaged skin (Kiistala, 1968). Microdialysis is another traditional time-consuming technique with the need of anesthesia professionals. The probe used for this technique needs calibration during the process and also results in trauma to the tissue (Bajramaj et al., 2019). Another technique is sonophoresis which uses vacuum pressure and low-frequency ultrasound to enhance skin permeability (Kost et al., 2000). However, the collection of ISF is difficult in this process as it spreads on the skin surface and a slight heat is produced on the skin (Maloney et al., 1992). Despite being an invasive approach, ISF extraction by microneedle patches causes minimal discomfort and minimizes the risk of blood contamination. ISF targeting microneedles are designed to reach the intracutaneous layer and prevent blood extraction (Taylor et al., 2020). These devices also contain minimally invasive needle heights ranging from 25 to 2000 μm. However, heights below 1000 μm are generally recommended as they tend to cause less pain (Luzuriaga et al., 2018).

Although microneedles are gaining interest among medical professionals and patients, their widespread use in healthcare is limited due to lengthy production times, high manufacturing costs, material limitations in different manufacturing techniques, and complex manufacturing processes. Traditional techniques for fabricating hollow microneedles such as micro drilling and deep reactive ion etching are time-intensive and costly (Bolton et al., 2020). Micromolding is also difficult due to the involvement of centrifugation or vacuuming steps (McGrath et al., 2014). Micromolding results in low resolution and mostly involves solid microneedle fabrication. However, the limitations of these conventional techniques can be overcome by the additive manufacturing (AM) techniques. Recently, research in tissue engineering and biomedical devices has explored the use of 3D printers, which can print at the micron scale (Economidou et al., 2018; Farias et al., 2018; Rahatuzzaman et al., 2024). Fused deposition modeling (FDM) is

* Corresponding author.
E-mail address: ejoyee@charlotte.edu (E.B. Joyee).

https://doi.org/10.1016/j.jmbbm.2025.107135
Received 30 April 2025; Received in revised form 28 June 2025; Accepted 10 July 2025
Available online 11 July 2025

an economical 3D printing technique that melts and extrudes thermoplastic materials, such as polylactic acid, at high temperatures. However, it has the drawback of low printing resolution in terms of manufacturing microneedle structures (Loh et al., 2024). Digital Light Processing (DLP), and Two-Photon Polymerization (2 PP) are technologies based on photopolymerization that form structures by curing UV-curable resin with UV light, providing high resolution (Layani et al., 2018). 2 PP is ideal for creating intricate and complex structures with a resolution of several hundred nanometers but it features a slow production rate and requires expensive equipment (Faraji Rad et al., 2021).

Traditional techniques for fabricating hollow microneedles such as micromolding, microdrilling, and deep reactive ion etching, often involve multi-step, time-intensive workflows, including fabrication of the master template, mold casting, curing (typically 2–4 h), and demolding. These steps not only extend production time but can also introduce various forms of geometric distortion and fabrication errors, especially when dealing with complex or hollow microstructures (McGrath et al., 2014). Moreover, micromolding lacks the resolution needed for high-precision edge features, limiting its suitability for refined microneedle geometries. To overcome some of these limitations, photopolymerization-based 3D printing methods, such as two-photon polymerization (2 PP), have been explored. These techniques provide exceptional resolution, often at the nanometer scale. However, 2 PP operates by scanning each structure point-by-point with a laser which makes it extremely slow and inefficient for producing large or detailed arrays. Faraji Rad et al. (2021) highlighted this trade-off, noting that while 2 PP offers excellent feature fidelity, its low throughput and long print durations severely restrict its practicality for high-volume and fast manufacturing. Cordeiro et al. (2020) reported that printing a 7 × 7 mm master template with 15 cross-shaped solid microneedles using 2 PP required approximately 43 h under optimized settings.

In our research, the hollow microneedle patch has been printed directly with a dimension of 8 × 3.3 mm with 8 microneedles of 1 mm height taking 4 h to print. The total material cost per patch is approximately $1.31, making it cost-effective for prototyping or clinical-scale use. Moreover, the μDLP process used in this study enables the direct of hollow microneedle (HMN) patches in a single step, without the need for mold preparation or secondary replication. The HMN patch shown in Fig. 5 was fabricated using the μDLP printer with a total runtime of approximately 4 h and total material cost per unit is approximately $1.31. This duration reflects the complete fabrication cycle from print initiation to final part readiness. While our current μDLP implementation does not support massive replication at the same scale as micromolding, it offers significant advantages in design flexibility (including patient-specific customization), rapid iteration, shorten process steps and high geometric fidelity particularly for hollow architectures that are challenging to reproduce through molding. The micro(μ) DLP based printing technique is comparatively economical and saves time while maintaining high resolution. Additionally, μDLP is advantageous for achieving smooth surface roughness and precise geometries, making it a better choice for applications that demand high-quality finishes. This technique minimizes the need for operator contact with the polymer during fabrication, ensuring the resin remains uncontaminated. Moreover, it guarantees precision and safety during production, further establishing μDLP as a superior option for high-resolution and efficient fabrication. Additive manufacturing techniques are influenced by the distinct properties of materials such as polymers, ceramics, metals, and alloys, which determine the process parameters and printed sample performances. Widely available homogeneous materials used for different AM techniques have some limitations in terms of fabricating microstructures. Achieving desired mechanical properties, structural integrity, thermal stability, dimensional accuracy, surface roughness is challenging for pure materials (Tan et al., 2020). Mixing ceramic material like silicon carbide (SiC) to the photocurable polymer can enhance the mechanical properties, structural integrity, dimensional accuracy and surface roughness (Yang et al., 2021). SiC as a ceramic filler material is a new challenge in terms of manufacturing hollow needles. Biocompatibility, non-toxicity, chemical inertness, and excellent mechanical strength make SiC a promising filler material for biomedical applications (Saddow, 2022). Its high stiffness and wear resistance enhances the mechanical stability of microneedles during skin insertion. Moreover, SiC's compatibility with photocurable resins supports uniform dispersion which enables the fabrication of robust composite structures using the μDLP process.

Besides the manufacturing process and material selection, the design and geometry of the microneedle play a crucial role. When it comes to extracting body fluids, several design criteria are important for microneedles. Key considerations in these designs include the angle of the microneedle, which affects ease of skin penetration, and the sharpness of the tip, which is critical for minimizing insertion pain and achieving effective fluid extraction. Additionally, the thickness of the needle walls and the overall structural integrity are crucial for ensuring mechanical stability during insertion. Surface smoothness is also important, as it can reduce friction and improve the ease of insertion. Various designs, such as conical, pyramidal, and snake fang shapes, focus on factors such as tip sharpness, insertion angle, internal channel dimensions, mechanical strength, skin penetration efficiency, and transdermal biological fluid extraction (Chang et al., 2017; Li et al., 2013; Mukerjee et al., 2004). For dermal sensing microneedles, the manufacturing precision should be less than 20 μm (Teymourian et al., 2021). For the dermal layer penetration, sharper needle tip requires less penetration force (Ahn, 2020). Römgens et al. revealed that for smooth skin penetration needle tip less than 15 μm is considered to be sharp (A.M. Römgens). Microneedles designed for fluid extraction will be based on capillary force. The length of the microneedles affects the capillary action, which is correlated to the extraction speed of dermal fluid (Samant and Prausnitz, 2018). Moreover, an important factor about the design criteria is the aspect ratio. Kochhar et al. found that a 2400 μm spacing microneedle array requires more force to penetrate the skin layer but achieves 20 % greater penetration compared to arrays with 800 μm spacing (Kochhar et al., 2013). Krieger et al. demonstrated the aspect ratio plays a vital role in mechanical strength of microneedle geometry (Krieger et al., 2019).

This study focuses on the design of an HMN inspired by the fountain pen structure, which will help optimize fluid extraction through enhanced capillary action and improved mechanical stability. By utilizing design elements such as a sharp tip and precise geometries, the microneedle can achieve efficient penetration and minimize insertion pain. Additionally, the incorporation of smooth surfaces and well-defined internal channels will further enhance the microneedle's performance in extracting ISF effectively.

New effective design inspiration, evaluating optimum printing parameters and print angle with respect to the build platform are important because of the micro features in the design. FEA software ANSYS Workbench 2022 R2 is used to evaluate the strength and deformation of the microneedles after load was applied on the HMN patch. Then a multimaterial μDLP printing technique is employed to fabricate the HMN patch with high resolution quality of 5 μm. Moreover, this study explores the challenge and feasibility of using SiC as a ceramic filler material for manufacturing hollow needles. The SiC nanoparticles are entrapped within the photopolymer matrix during the μDLP curing process. The cross-linked polymer network forms a rigid, continuous structure in which SiC particles are not free to migrate. Manufacturing an HMN patch using silicon carbide polymer composite with μDLP presents several challenges, including material shrinkage during curing and post-processing, rough surfaces after printing, difficulty in removing support structures, and achieving maximum material densification. A smooth surface is crucial to minimize patient discomfort, making it one of the key factors in the design. Optimizing curing time and layer thickness is essential in the manufacturing process. Proper curing ensures material solidification as intended; over-curing can cause excessive shrinkage, while under-curing may lead to incomplete polymerization and weak structures.

In μDLP, the curing time for each layer must be optimized according to the material, geometry, and thickness to prevent distortion and printing failures. Additionally, thinner layers improve resolution, surface smoothness, and detail accuracy, which are critical for micro-scale printing with polymer-ceramic composites. However, reducing layer thickness increases total print time and may impact the curing process. Therefore, fine-tuning layer thickness is essential to ensure that small features, such as sharp angles or thin walls, are accurately reproduced.

2. Materials and method

2.1. Design inspiration and methodology

The HMN manufacturing with silicon carbide begins with the design inspiration, which is then converted into a computer aided design (CAD) geometry. A finite element analysis (FEA) was conducted on the CAD model using the properties of the polymer, followed by fabrication using the μDLP technique. The analysis is performed to simulate and predict the structural behavior, to validate the feasibility of the design. Once validated, the microneedle patch was designed using CAD software and exported as a standard tessellation language (STL) file for slicing and printing.

The microneedles are then fabricated at specific print angles with a goal to retain the CAD design shape. Once the optimal print angle is achieved and the fabricated samples meet the requirements, the manufacturing process involves SiC as filler ceramic material. Fig. 1 represents the schematic of the methodology followed for the study.

2.2. Materials

In this study, a modified μDLP printer with 365 or 385 nm adjustable UV power source was used. The baseline printer used in this study is a Kudo3D MicroDLP system, which is ideal for printing photo sensitive polymer resin. The optical setup, including the light penetration glass thickness and DMD chip of the machine was modified. These changes were made to optimize the system for printing ceramic particle loaded resins by adjusting the light parameters. Regarding the long-term cost and throughput considerations, this study primarily focuses on the design and geometric optimization of hollow microneedle structures for extracting interstitial fluid. The DLP system is demonstrated in Fig. 2b. For the printing process, a high-resolution photopolymer resin called 3DSR UHR by Kudo3D was purchased. It has a density of 1.1 g/cm^3, a viscosity of 330 cP, and a tensile strength of 29.2 MPa. This photocurable polymer is capable of producing extremely fine details, with the ability to print features as small as 5 μm. Although the 3DSR UHR used in this study is not inherently biocompatible, it was chosen for its excellent printability with the current μDLP setup. Once the design is finalized, a biocompatible polymer resin with similar rheological and mechanical properties will be tested to fabricate biocompatible patches. SiC nanopowder (Beta SiC, 99 %, <80 nm, cubic, US Nano, TX, USA) was mixed with the 3DSR. Parafilm (thickness 0.127 mm) was purchased to be used as model skin to examine the microneedles perforation, and a DSX1000 Digital Microscope was used to take images of the printed samples and measure the bending angles of the samples due to different printing orientations.

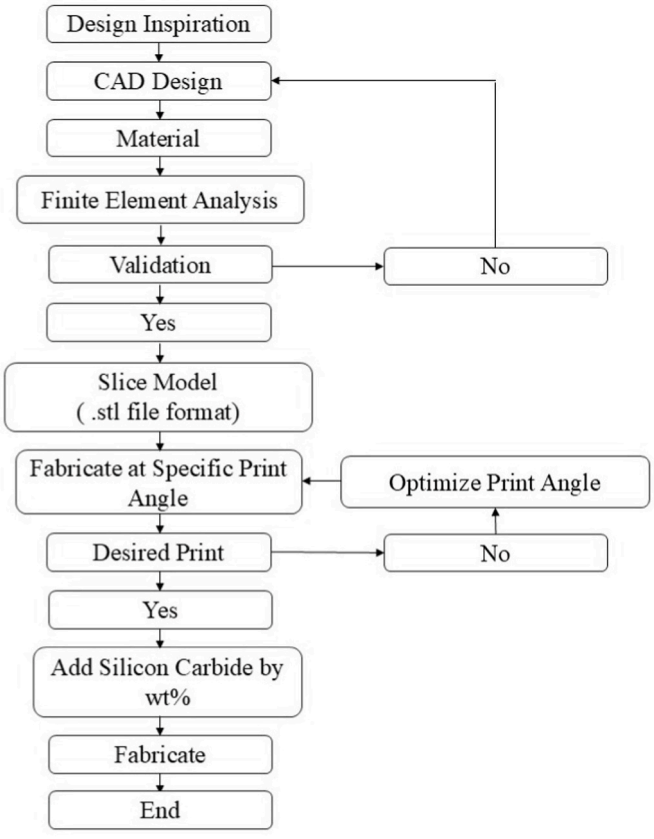

Fig. 1. Schematic of the research methodology.

2.3. Design inspiration

Nature has consistently provided inspiration for researchers in developing design approaches that yield unique and enhanced properties for different purposes like designing hierarchical structure, biomedical devices, bioinspired actuators etc. (Joyee et al., 2020; Khecho and Joyee, 2024; Rahman and Joyee, 2022). Microneedle patches for different applications have drawn inspiration from a diverse array of natural organisms. For example, Zhang et al. designed microneedles for sustained drug delivery with antibacterial properties based on the suction cups of octopus tentacles (Zhang et al., 2020). In another study of Zhang et al., the hierarchical microstructure of gadflies, ladybugs, and the feet or stings of wasps were used as a guideline for microneedle design for adhesion and rapid hemostasis through a multilayered structure, ideal for emergency bleeding control (Zhang et al., 2021).

In this study, the structure of plant roots and stems were utilized as inspiration for the extraction of ISF fluid from the mammalian dermal tissue. Wu et al. mentioned HMN extraction of ISF through a suction mechanism facilitated by capillary action (Wu et al., 2022). This capillary action force is similar to the mechanism of plant roots for absorbing water from the soil (Raats, 2007). The developed microneedle patch in this study is designed to function similarly to plant roots, effectively collecting fluid through capillary action, which can also be analogous to that found in fountain pens. Plant root hairs receive all nutrients including water from soil via capillary action across highly porous, narrow tissue channels. This approach is efficient and passive. Inspired from this biological mechanism, a capillary-assisted ISF extraction within our microneedle's hollow lumen was designed. The tapered shape of the HMN (Fig. 2c), along with potential of surface treatments to increase hydrophilicity, are designed to enable fluid absorption from the dermis without pressure. The taper shape of the HMN was inspired by the geometry of a fountain pen, which also enables a fluid-guiding architecture. As shown in Fig. 2c, the longitudinal slit in traditional nibs enables capillary flow from the ink reservoir to the paper during writing (Nikolov et al., 2020), while the functional mechanism of our HMN differs employing an enclosed lumen rather than a slit. Microneedle design in this study mimics the tapered shape and centralized flow pathway but replaces the open slit with an enclosed lumen to facilitate directed fluid uptake from the dermis. The functional mechanism of the microneedle matches with the capillary action of the plant root (Fig. 2c), while the geometrical architecture follows the working principle of a fountain pen nib. Fig. 2 demonstrates a side-by-side mapping of the

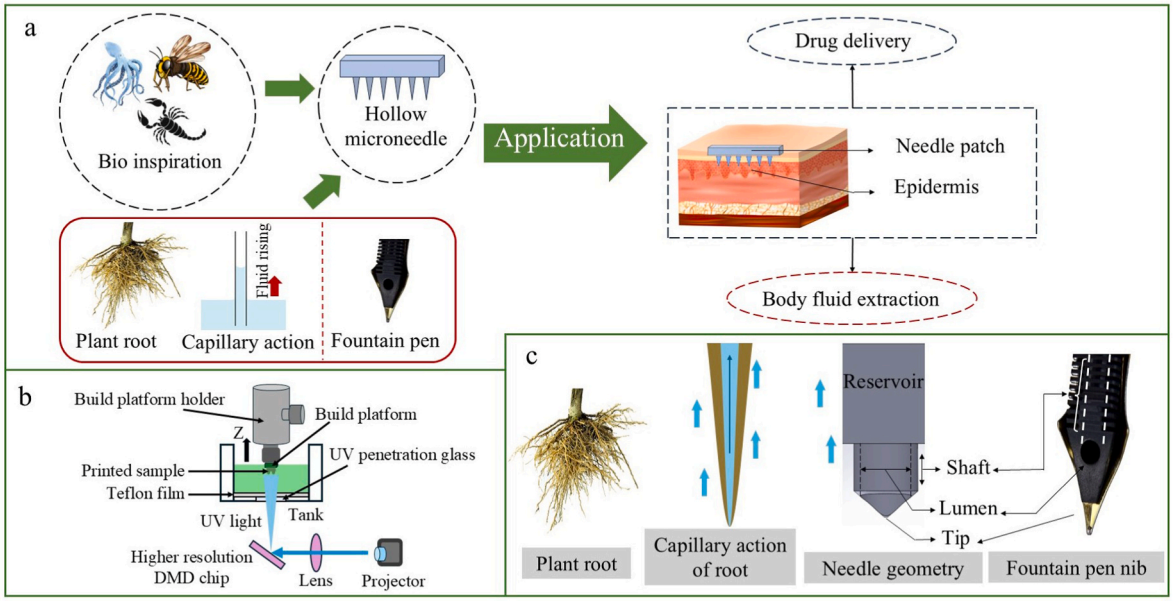

Fig. 2. (a) Fountain pen design inspiration of the needle patch; (b) Modified μDLP printing process; (c) Plant root capillary action and needle geometry inspiration from fountain pen nib.

capillary effect inspired by the plant roots and various parts of the microneedle design, which are modeled after a fountain pen nib. Based on a thorough analysis of prior research (Samant et al., 2020) and the specific requirements for microneedles relative to the thickness (>100 μm) of the target skin layer, a hollow microneedle patch has been designed in this study. Fig. 2a,c illustrates the inspirations behind the microneedle design and its intended applications.

2.4. CAD geometry

The CAD model of the proposed HMN was developed using SolidWorks (Dassault Systems SOLIDWORKS Corp.), Version 2024, Massachusetts, USA. Fig. 4 shows the CAD geometry of the HMN patch including the different parts of the model. The design of the HMNs for ISF extraction involves microscale features and precision manufacturing techniques. This extraction device consists of an array of 4 × 2 orders (Fig. 3a). The cross-sectional view (Fig. 3b) of the HMN array shows each microneedle has 1 mm height above a 0.355 mm thick base, ensuring optimal skin penetration with minimal discomfort. Studies have demonstrated that longer microneedles are associated with increased pain upon application, as they are more likely to interact with pain receptors (Turner et al., 2021). A 0.480 mm long hypodermic needle produces 5 % of the pain response, while increasing the length to 1.45 mm results in the pain response to 37 % (Gill et al., 2008). The reservoir of the HMN patch has dimensions of 8 mm × 3.33 mm × 1 mm (Length × Width × Height). The top-view (Fig. 3a) layout of the microneedle array displays the hollow lumen of 0.8 mm diameter, and the microneedle outlet diameter is 1 mm with a tip diameter of 50 μm. The tip diameter under 75 μm is suitable for avoiding pain and effectively puncturing the skin (Luzuriaga et al., 2018).

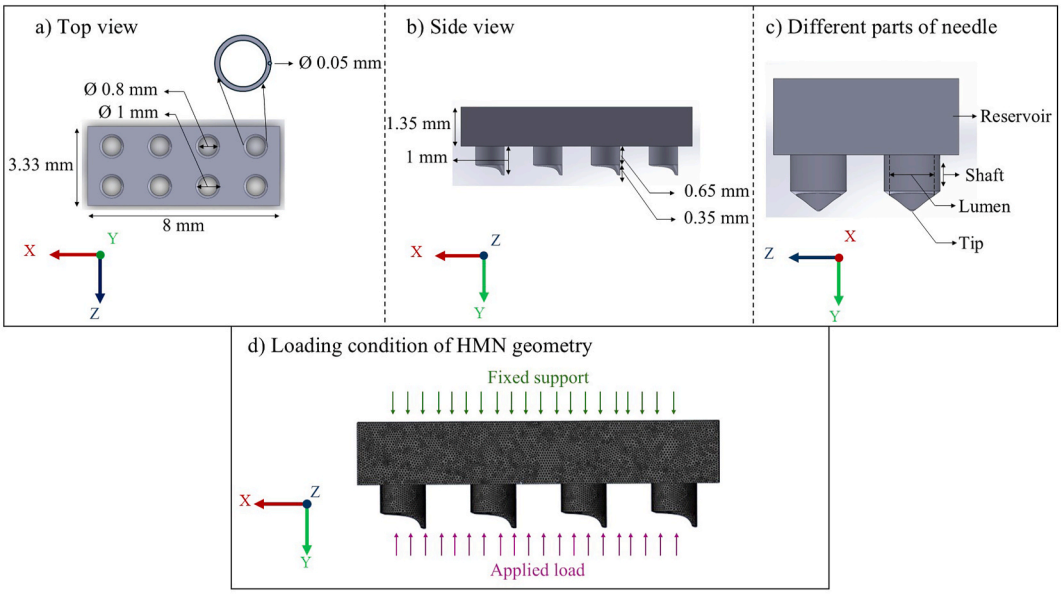

Fig. 3. (a) Top view; (b) Side view; (c) Different parts of the needle; (d) Loading condition of HMN geometry.

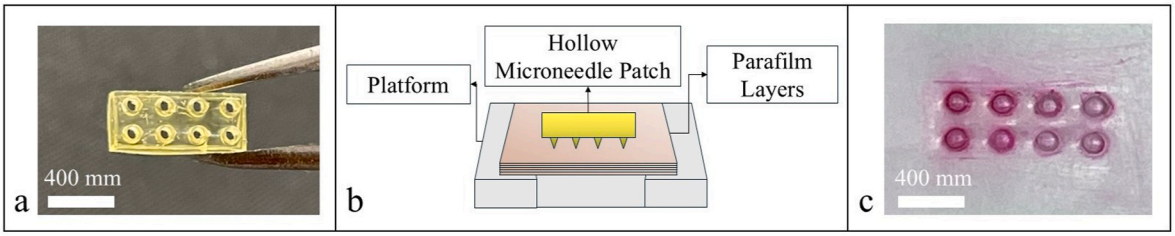

Fig. 4. (a) The printed HMN; (b) HMN insertion test setup; (c) Pierced marks on Parafilm layers from the penetrated HMN patch.

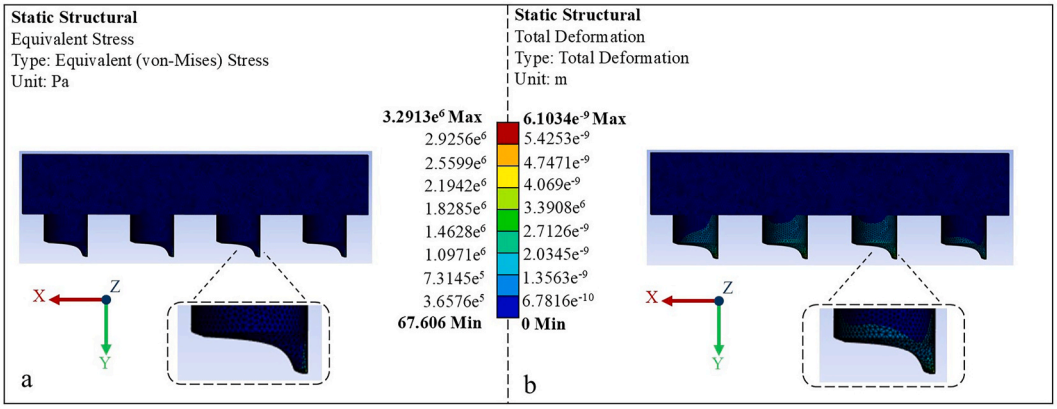

Fig. 5. Simulation result at true scale. (a) Equivalent von-Mises stress of HMN patch; (b) Total deformation of the HMN patch.

2.5. Finite element analysis

2.5.1. Mesh

FEA is a mathematical technique used to evaluate the behavior of physical systems. In this study, ANSYS Workbench 2022 R2 was used to generate mesh for the microneedle geometry. A high-detailed mesh is essential for accurately simulating physical events. On the other hand, a coarse mesh may lead to convergence issues, resulting in incorrect interpretations and inaccurate results (Okereke and Keates, 2018). For this analysis, a tetrahedral mesh with a size of 0.00005 was employed to the CAD geometry.

2.5.2. Boundary condition

Boundary conditions are parameters applied to a model to simulate the real-world interactions and limitations on a structure. It defines how external forces, displacements, or fixed supports influence its behavior under specific conditions. A pressure of 3.183 MPa was applied to the tip of the microneedle patch along the z-direction, as this level of pressure is necessary to penetrate human skin (Henry et al., 1998). The bottom surface was considered to be fixed to run the simulation. The total deformation (δ_{total}), and equivalent von-Mises stress (σ_v) were analyzed in the FEA analysis following equation (1):

$$\sigma_v = \sqrt{\frac{(\sigma_1 - \sigma_2)^2 + (\sigma_2 - \sigma_3)^2 + (\sigma_3 - \sigma_1)^2}{2}} \quad (1)$$

equation (1) shows the formula for calculating the von Mises stress, σ_v, which is a scalar value derived from the principal stresses σ_1 , $\sigma 2$ *and* $\sigma 3$. This comprehensive method helped us to replicate the real-life conditions and better comprehend how microneedles responded to different load conditions. Fig. 3d demonstrates the loading condition and fixed support of the HMN geometry.

The initial step in manufacturing a 3D HMN patch involves designing a CAD file inspired by the design of a fountain pen. This CAD file is imported into 3D Builder (Microsoft, USA) to verify its printability at the micrometer scale based on the voxel size. Following this verification, Kudo3D software is used to slice the CAD model, preparing it for the printing process. A modified μDLP printer is then utilized to print the HMNs according to the specified features outlined in the CAD model. During the printing process, various orientations are considered to optimize the fidelity of the printed model.

2.6. Insertion test

For the insertion test, a Parafilm with a thickness of 0.127 mm was used. There is a notable similarity in mechanical properties between the layers of Parafilm film and porcine skin. The Young's modulus of Parafilm is 30–60 MPa and 56–111 MPa for porcine skin. Based on this, simple insertion tests can be reliably conducted on Parafilm (Larrañeta et al., 2014). Each layer of Parafilm measures 127 μm, and the film is folded into eight layers to achieve an approximate total thickness of 1 mm. The HMN array is subsequently inserted through the eight layers of the membrane using a setup that incorporates a REB7-001M-S force sensor from Loadstar Sensors. The insertion test apparatus is illustrated in Fig. 4.

2.7. Composite materials in enhancing microneedle performance

For ISF extraction, the mechanical properties of microneedles are critical; they should possess an optimal balance between rigidity and softness. Microneedles that are too rigid may cause unnecessary discomfort and tissue damage upon insertion, while those that are excessively soft may not effectively penetrate the skin, compromising their ability to extract ISF. Therefore, the development of composite materials presents a promising solution for microneedle fabrication. By combining different materials, it is possible to achieve a tailored mechanical profile that enhances performance characteristics. Composite materials can be engineered to provide the necessary strength for structural integrity while maintaining sufficient flexibility to minimize pain and trauma during application. This adaptability makes composite microneedles an ideal candidate for efficient ISF extraction, improving patient comfort and procedural efficacy.

2.7.1. Silicon carbide polymer composite preparation

The ceramic resin was prepared by mixing the SiC with a photocurable polymer. A homogenous solution of SiC nanoparticles and photocurable polymers was made with six different weight percentages (1 %, 3 %, 5 %, 10 %, 15 %, and 20 %) of SiC particles. The mixing process was conducted in two steps to eliminate particle agglomeration. In the first step, SiC and polymer were mixed using a magnetic stirrer for 5 min. Subsequently, ultrasonication was done for 10 min with pulse setting of 5 s to ensure that the ceramic nanoparticles are evenly dispersed throughout the solution. Initially different weight ratios of SiC and polymer were prepared to print cube shaped samples measuring 3 mm × 3 mm × 0.375 mm (Length × Width × Height). Following the successful printing of these cube structures with various compositions of ceramic and polymer, the microneedle patch was printed with different weight percentage ratios of SiC and polymer.

2.7.2. Rheological properties

Rheological properties in ceramic resin are essential for controlled flow, uniform particle distribution, and precise curing. These properties are crucial for achieving high-quality, defect-free prints. They directly impact on the resin's printability, stability, and final mechanical properties of ceramic parts. The flow behavior of the ceramic polymer composite was evaluated by Discovery HR-10 Rheometer (TA Instruments, Inc. USA) with a 20 mm parallel plate geometry for the μDLP printing technique. The shear stress versus shear rate and the viscosity versus shear rate curves were generated through a flow ramp test. The tests were conducted at room temperature, with shear rates ranging from 0.1 to 1000 s^{-1} and a parallel plate gap of 0.5 mm.

3. Results and discussion

3.1. Finite element analysis results

FEA is an effective simulation based mechanical analysis, especially for evaluating stresses and deformations in solid structures. This approach simplifies the result prediction of complex physical models. In addition to that, a finer FEA mesh provides simulation results closer to real-life predictions. The results from the simulation (Fig. 5a), show the results of a static structural analysis performed in ANSYS, highlighting the equivalent von-Mises stress distribution in a HMN patch. The stress distribution ranges from a minimum of 67.606 Pa to a maximum of 3.291 MPa. In a similar type of research Ahmad et al. reported that for the axial load of 3.18 MPa, the maximum von-Mises stress was observed to be 3.4 MPa and the total deformation was 0.81 μm for hollow microneedles (Ahmad et al., 2021). Anbazhagan et al. reported a maximum stress of 3.02 MPa for the conical microneedle and slightly below 3.16 MPa for the pyramidal microneedle under axial loading conditions (Anbazhagan et al., 2023). Compared with these prior findings the stress analysis result indicates that the microneedle patch possesses a higher compressive load capacity.

Simultaneously, the simulation in this research illustrates the deformation of the model in Fig. 6b. The total deformation ranges from a maximum value of 6.1034×10^{-9} to a minimum value of 6.7816×10^{-10}. The microneedle has a total length of 1000 μm according to the CAD model, with a maximum deformation measured at 6.1034×10^{-9} m, which is negligible in comparison to the microneedle's length. Fig. 5 is the representation at true scale without any artificial scaling or visual exaggeration of simulation result.

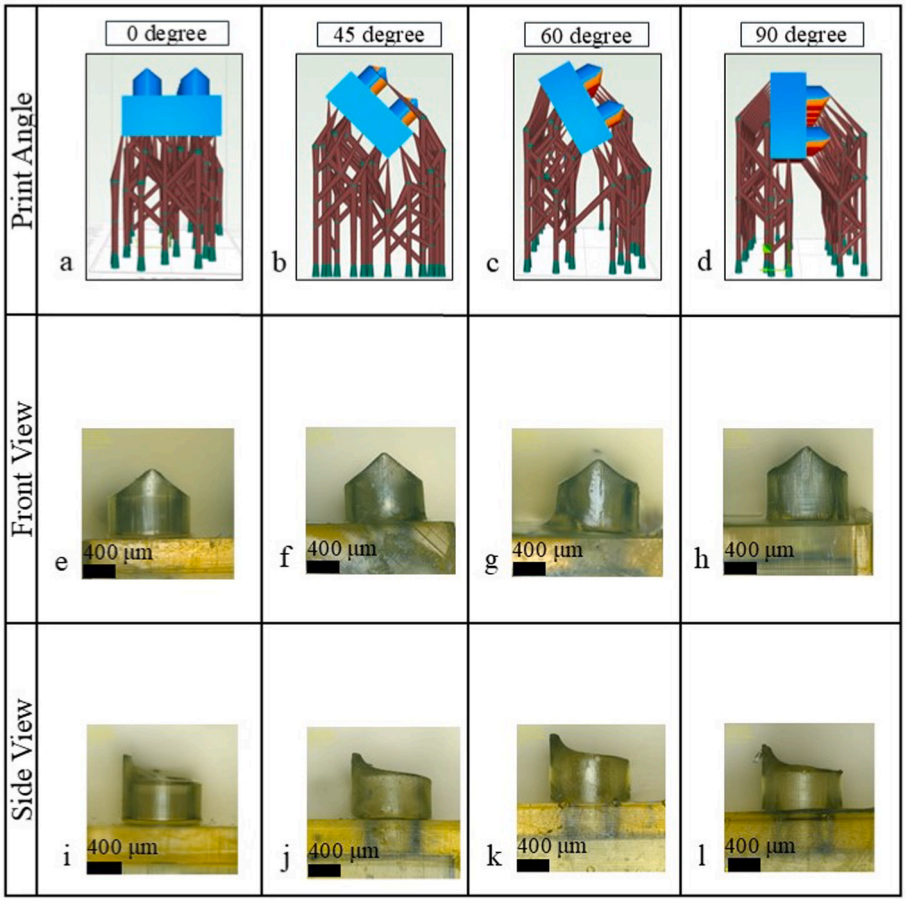

Fig. 6. (a, b, c, d) HMNs in different printing angles; (e, f, g, h) Front view; (i, j, k, l) Side view.

3.2. Fabricated HMNs in various angles

Fig. 6 illustrates the sliced model with a support structure to manufacture 3D HMN patches by varying the print orientations. A modified μDLP printer was used to print the HMNs, with four different orientations—0, 45, 60, and 90°. These orientation angles were considered to find the optimal print quality. Fig. 6a-d represent the 3D models with support structures for each orientation, while Fig. 6e-h and Fig. 6i-l show the front and side views of the printed microneedles, respectively. For the geometry printed at 0, 45, 60, and 90-degree angles, the number of layers was 1371, 1704, 1712, and 1566, respectively. The LED exposure time was set to 12 s for the first 2 layers, 10 s for layers 3 to 5, 6 s for layers 6 to 10, and 5 s from layer 11 to the last layer of the sample for each print angle model. The exposure time for the initial layers was set to 12 s for optimal adhesion of the cured resin to the build platform. The printed samples at 0 and 90-degree angles successfully retained the structure of the CAD model. On the other hand, the 45 and 60-degree angles resulted in tilted printing of the CAD model geometry. Between the 0 and 90-degree print angles, the 0-degree orientation provided a better printed microneedle. Alternatively, the 90-degree orientation needed to have more support structures to retain the shape of the microneedle. But it could not avoid the geometric deformities that can be seen from Fig. 6l. After successful prints, a post-curing process of 10 min was performed for all printed patches.

The front and side views illustrate differences in surface finish and structural integrity across various printing angles. They also demonstrate the effects of support structures on these features. This analysis emphasizes the critical role of print orientation in achieving optimal print quality. The needle length of 1 mm ensures minimal discomfort with comparatively less pain. The tip diameter of 5 μm will help the HMN patch penetrate the dermal layer comfortably. Moreover, from the CAD model, the needle shaft length was designed for capillary action to extract the ISF like how plant roots absorb water.

3.3. Insertion test results

In order to evaluate the performance of the microneedles, Parafilm was chosen for its mechanical behavior closely matching the porcine skin. To identify the penetration depth of the microneedles, a dye solution made of Rose Bengal powder and ethanol was used. A force sensor and loadstar sensors DS-3000-Pro4 touch screen display configuration evaluated the penetration force test results. A total number of 4 replications were done with two volunteers. Each insertion test was conducted for 10 s before the microneedles were removed from the Parafilm. The layers of Parafilm were individually evaluated, producing the results shown in Fig. 7.

Force applied below 15 ± 0.5 N was considered to be low force and above 15 ± 0.5 N was high force. For applied forces ranging from 3 ± 0.5 N to 15 ± 0.5 N, the microneedles penetrated a single layer of the Parafilm model, leaving discernible needle imprints on the subsequent three to four layers. When the applied force was increased to the range of 20 ± 0.5 N to 30 ± 0.5 N, two layers were fully penetrated by the microneedles, with visible imprints observed on the fifth and seventh layers of the Parafilm stack. As a result, the range of force between 20 ± 0.5 N and 30 ± 0.5 N reached the target area filled with ISF. This progressive increase in penetration depth with higher applied forces highlights the effectiveness of HMN in simulating the impact of varying insertion forces on microneedle penetration depth. Insertion of the microneedle patch can cause pain, which is evaluated along with its ability to penetrate the skin. The dimensions of the microneedle presented in Fig. 3 slightly exceed the dimensions of shorter-gauge hypodermic needles (e.g. 26G). However, prior studies, such as Gill et al. (2008), have shown that microneedles up to 1450 μm in length produce only 37 % of the pain reported with a standard hypodermic needle. The 1000 μm height used here is deep enough to reach interstitial fluid, but shallow enough to minimize activation of dermal nociceptors (pain receptors). In another research, Turner et al. (2023) manufactured a microneedle patch where each needle is of 1 mm width and 1 mm height successfully extracted dermal fluids. The primary focus of this study is to demonstrate a capillary-based fluid extraction mechanism using a rigid microneedle architecture. The dimensions were selected to validate the functionality of the proposed design using the μDLP fabrication process. Nonetheless, the resolution of the μDLP system allows for future scaling of the microneedle size to smaller, and less invasive geometries as needed.

3.4. Rheology behavior

Fig. 8 represents the rheological behavior of homogeneous polymers mixed with different weight percentages of SiC (1 %, 3 %, 5 %, 10 %, 15

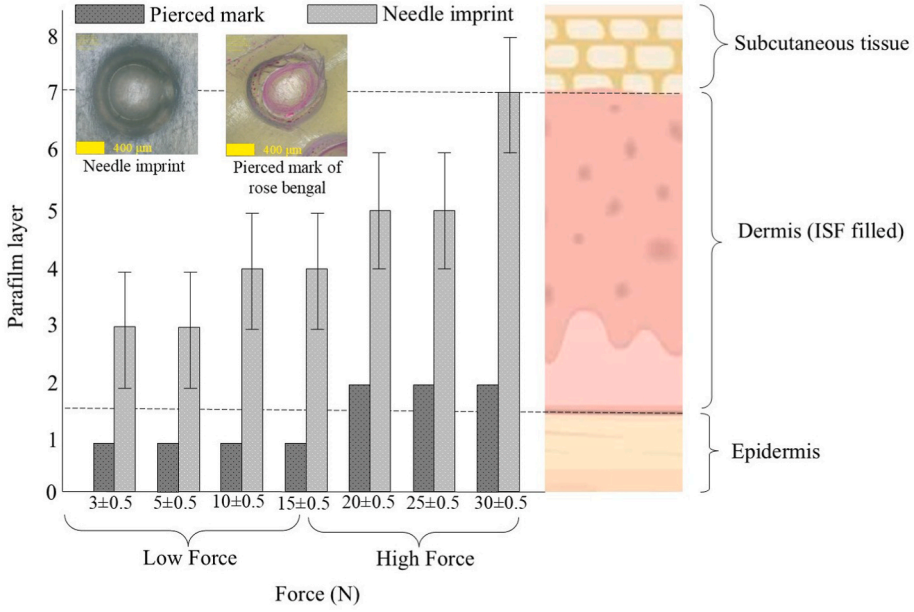

Fig. 7. Relation between penetration force and parafilm layers.

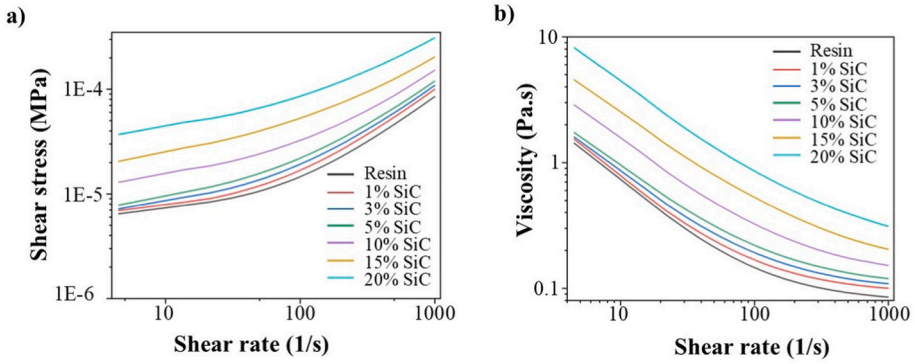

Fig. 8. Flow characteristics of the SiC-polymer composite; a) The relationship between shear stress and shear rate; b) Viscosity change with shear rate.

%, and 20 %). The data illustrates the effect of increasing SiC concentration on shear stress and viscosity as a function of shear rate. Increasing the amount of SiC resulted in increased shear stress for a given shear rate. It was observed that in higher SiC concentrations of 15 % and 20 %, the flow resistance increased significantly. This indicates that adding more SiC significantly raised the flow resistance of the material. With the rapid increase in shear stress, a higher SiC content produced a more significant rise. The homogeneous polymer exhibited the lowest shear stress across all shear rates.

Conversely, the viscosity decreased as the shear rate increased, demonstrating typical shear-thinning behavior for such composites. With increasing SiC content, the overall viscosity was higher at the given shear rate. For instance, the material with 20 % SiC exhibited the highest viscosity, while the homogeneous polymer showed the lowest. The curves followed a similar downward trend, with increasing shear rates reducing viscosity across all SiC polymer-composite mixtures. This effect was especially prominent in higher SiC contents.

3.5. Printing HMN patch with silicon carbide polymer composite

The incorporation of SiC altered the rheological properties of the composite polymers used for manufacturing HMN via the μDLP technique. It is essential to assess the feasibility of printing small, detailed structures at higher SiC weight percentages within the polymer matrix. To examine this, a series of cube structures were printed with varying SiC concentrations. For SiC weight percentages of 1 % and 3 %, the curing time was set to 6 s per layer with a 5 μm thickness, similar to the curing time required for the homogeneous polymer. In contrast, for SiC concentrations of 5 %, 10 %, 15 %, and 20 %, the curing times increased to 8, 10, 12, and 15 s per layer, respectively. This indicates that higher SiC content necessitates longer curing times to achieve adequate layer solidification. Fig. 9 illustrates the successfully printed cube structures with varying curing times.

After integrating SiC, adjustments in curing time were required to ensure the structural integrity of the printed composites. Although cube structures were successfully fabricated, the needle geometry presented challenges due to issues like sedimentation, viscosity changes during printing, and light scattering caused by SiC's optical properties. In Fig. 10a-d, the front and side views of microneedles printed with 1 % and 3 % SiC demonstrate well-defined geometries. To date, HMN patches have been successfully printed with 1 % and 3 % SiC content. The front view reveals a sharp, uniform tip, while the side view shows a smooth, consistent curvature, indicating proper layer adhesion and curing with no structural irregularities. These observations are consistent with those obtained from the printed cube structures across varying SiC concentrations.

Increasing the SiC content introduced light scattering and pigment darkening effects, both of which reduce UV penetration and increase effective curing time. Specifically, full patch microneedles without filler printed in about 4 h, while those with 1 wt% and 3 wt% SiC took around 4 h 12 min and 4 h 15 min, respectively. The total manufacturing time is less than the 2 PP technique. All curing is performed through the μDLP system itself, followed by a short UV post-curing step to remove any residual resin after cleaning from the printed parts. No additional thermal or curing methods were used for post processing. The total curing time scales linearly with the number of layers, since each layer is exposed sequentially. For example, the MN patch shown in Fig. 4, which consists of approximately 800 layers, was printed in 4 h using DLP, followed by 10 min of UV post-curing at room temperature. As the SiC content increased, each layer needed more exposure time due to increased light scattering and reduced penetration depth. Light intensity and exposure settings were adjusted to ensure adequate polymerization, eliminating the need for additional post-processing to address the filler's scattering effects.

Fig. 10 also provides detailed imaging of the printed microneedles. Fig. 10e represents the successfully printed HMN patches, with the homogeneous polymer shown on the left and the ceramic-polymer composite on the right. The magnified SEM image (Fig. 10f) of 3 % SiC microneedle displays overcuring was evident. The intended wall thickness of the microneedle was 0.2 mm, but the printed sample shows a wall thickness of 0.253 mm, indicating an overcuring effect of 0.053 mm. Additionally, Fig. 10g reveals that the tip diameter increased to

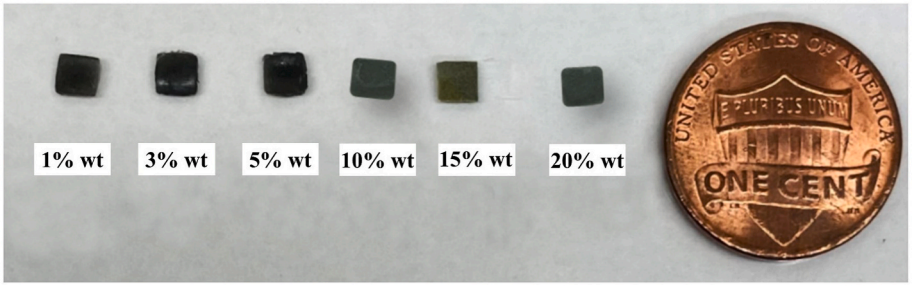

Fig. 9. SiC-polymer composite 3D printed cube shapes.

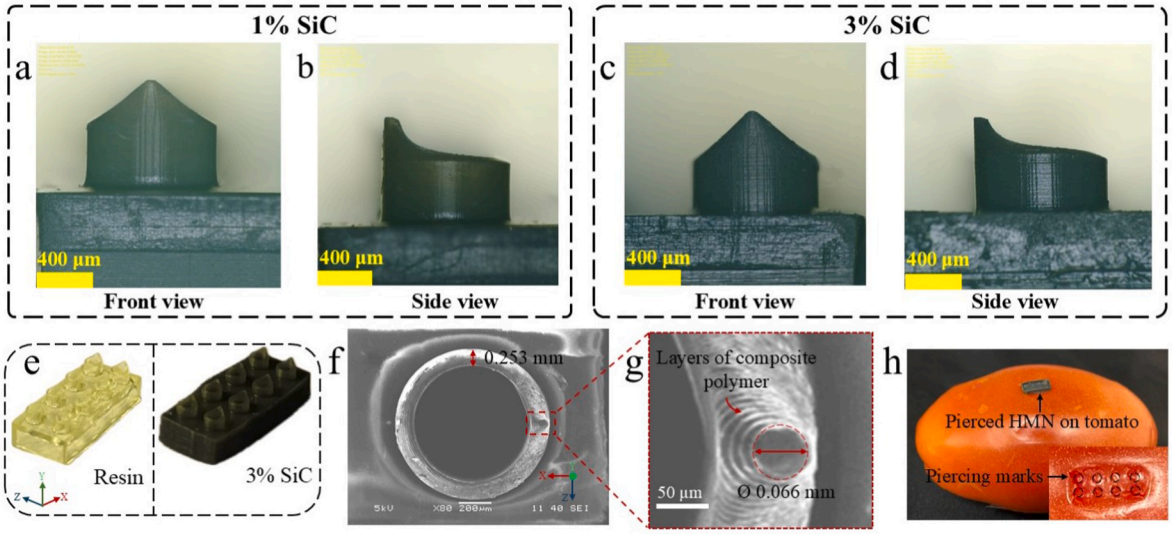

Fig. 10. (a, b) 1 % SiC printed HMN; (c, d) 3 % SiC printed HMN SiC; (e) Resin and SiC printed HMN; (f) SEM image top view of 3 % SiC HMN; (g) SEM magnified top view of HMN tip; (h) Piercing HMN on tomato.

0.066 mm from the designed 0.05 mm. This was because the high viscosity of the SiC-polymer composite slurry and change of color of the homogenous polymer for adding SiC caused additional light absorption and influencing the curing process. Moreover, as shown in Fig. 10h, the HMN patch was applied on the tomato skin to evaluate the sharpness of the needle and penetration marks. After the post-curing process, no exposed or loosely bonded SiC particles were observed on the HMN surface. Microscopic (Fig. 10a-d) and SEM imaging (Fig. 10f-g) confirm that the nanoparticles are physically entrapped within the polymer matrix. While direct immersion in ISF was not performed, the absence of particle release under simulated use conditions (e.g. insertion into Parafilm and tomato skin) demonstrated robust particle retention. The Parafilm insertion left clean puncture marks without residue, and the tomato skin exhibited defined insertion points with no sign of exposing SiC nanoparticles around the puncture area. The strong particle-polymer bonding observed in the SEM analysis implies that SiC leakage into body fluids is unlikely. This has significant implications for the biocompatibility and long-term safety of the microneedle patch. However, future studies will include immersion testing in simulated interstitial fluid environment.

4. Conclusions

The objectives of this research were to design, fabricate, and integrate SiC for fabricating HMN while determining optimal printing parameters for µDLP manufacturing. Additionally, the study evaluated the effect of print angle relative to the build platform to achieve the highest print quality. FEA was conducted on homogeneous polymer material to predict microneedle performance prior to fabrication, ensuring feasibility. The penetration tests confirmed the functional integrity of the HMNs, demonstrating their effectiveness in practical applications. This study also introduces SiC as a reinforcing material to enhance the structural strength of HMNs. Hollow microneedles are increasingly utilized for applications such as body fluid extraction and drug delivery, where surface smoothness, durability and precision are essential. The novelty of this research lies in the HMN design, inspired by fountain pen geometry and the innovative use of SiC-polymer composite to manufacture sharp, durable microneedles. This approach offers a promising advancement in the field of HMN fabrication, combining design innovation with enhanced material properties for improved functionality.

5. Future works

Future work will aim to optimize the SiC weight ratio in the polymer composite to achieve the highest feasible weight percentage for HMN fabrication. Subsequent studies will involve a comprehensive evaluation of the mechanical properties of HMN patches printed with varying SiC-polymer composite ratios. Finally, the fabricated HMN patches will undergo surface coating to enhance hydrophilicity, followed by biocompatibility testing to ensure suitability for the extraction of target body fluid. To evaluate the stability of the SiC-polymer composite, the HMN samples will be immersed in a simulated interstitial fluid (ISF) environment to assess potential material degradation or leaching of SiC particles. This will help determine whether the SiC remains embedded within the microneedles or if there is any risk of particle release. Besides, different dimensions of the design will be tested following the protocol discussed in this research.

CRediT authorship contribution statement

Md Rahatuzzaman: Writing – original draft, Methodology, Investigation, Data curation, Conceptualization. **Erina Baynojir Joyee:** Writing – review & editing, Validation, Supervision, Resources, Investigation, Funding acquisition, Formal analysis, Conceptualization.

Declaration of competing interest

The authors declare no competing interests.

Acknowledgement

No financial competing interest exists for any author.

Data availability

Data will be made available on request.

References

Ahmad, N.N., Ghazali, N.N.N., Wong, Y.H., 2021. Mechanical and fluidic analysis of hollow side-open and outer-grooved design of microneedles. Mater. Today Commun. 29, 102940. https://doi.org/10.1016/j.mtcomm.2021.102940.

Ahn, B., 2020. Optimal microneedle design for drug delivery based on insertion force experiments with variable geometry. Int. J. Control Autom. Syst. 18, 143–149. https://doi.org/10.1007/s12555-019-0220-8.

Anbazhagan, G., Suseela, S.B., Sankararajan, R., 2023. Effect of hollow microneedle geometry structure on mechanical stability and microfluidic flow for transdermal drug delivery applications. Microfluid. Nanofluidics 27, 25. https://doi.org/10.1007/s10404-023-02636-5.

Bajramaj, E., Häggman-Henrikson, B., Dawson, A., Gerdle, B., Ghafouri, B., 2019. The effect of microdialysis catheter insertion on glutamate and serotonin levels in masseter muscle in patients with myofascial temporomandibular disorders and healthy controls. Diagnostics 9, 14. https://doi.org/10.3390/diagnostics9010014.

Bolton, C.J.W., Howells, O., Blayney, G.J., Eng, P.F., Birchall, J.C., Gualeni, B., Roberts, K., Ashraf, H., Guy, O.J., 2020. Hollow silicon microneedle fabrication using advanced plasma etch technologies for applications in transdermal drug delivery. Lab Chip 20, 2788–2795. https://doi.org/10.1039/D0LC00567C.

Chang, H., Zheng, M., Yu, X., Than, A., Seeni, R.Z., Kang, R., Tian, J., Khanh, D.P., Liu, L., Chen, P., Xu, C., 2017. A swellable microneedle patch to rapidly extract skin interstitial fluid for timely metabolic analysis. Adv. Mater. 29, 1702243. https://doi.org/10.1002/adma.201702243.

Cordeiro, A.S., Tekko, I.A., Jomaa, M.H., Vora, L., McAlister, E., Volpe-Zanutto, F., Nethery, M., Baine, P.T., Mitchell, N., McNeill, D.W., Donnelly, R.F., 2020. Two-photon polymerisation 3D printing of microneedle array templates with versatile designs: application in the development of polymeric drug delivery systems. Pharm. Res. 37, 174. https://doi.org/10.1007/s11095-020-02887-9.

Economidou, S.N., Lamprou, D.A., Douroumis, D., 2018. 3D printing applications for transdermal drug delivery. Int. J. Pharm. 544, 415–424. https://doi.org/10.1016/j.ijpharm.2018.01.031.

Faraji Rad, Z., Prewett, P.D., Davies, G.J., 2021. High-resolution two-photon polymerization: the most versatile technique for the fabrication of microneedle arrays. Microsyst. Nanoeng. 7, 71. https://doi.org/10.1038/s41378-021-00298-3.

Farias, C., Lyman, R., Hemingway, C., Chau, H., Mahacek, A., Bouzos, E., Mobed-Miremadi, M., 2018. Three-dimensional (3D) printed microneedles for microencapsulated cell extrusion. Bioengineering 5, 59. https://doi.org/10.3390/bioengineering5030059.

Gill, H.S., Denson, D.D., Burris, B.A., Prausnitz, M.R., 2008. Effect of microneedle design on pain in human volunteers. Clin. J. Pain 24, 585–594. https://doi.org/10.1097/AJP.0b013e31816778f9.

Henry, S., McAllister, D.V., Allen, M.G., Prausnitz, M.R., 1998. Microfabricated microneedles: a novel approach to transdermal drug delivery. J. Pharmaceut. Sci. 87, 922–925. https://doi.org/10.1021/js980042+.

Joyee, E.B., Szmelter, A., Eddington, D., Pan, Y., 2020. Magnetic field-assisted stereolithography for productions of multimaterial hierarchical surface structures. ACS Appl. Mater. Interfaces 12, 42357–42368. https://doi.org/10.1021/acsami.0c11693.

Khecho, A., Joyee, E.B., 2024. Design and fabrication of bioinspired pattern driven magnetic actuators. Funct. Compos. Struct. 6, 015010. https://doi.org/10.1088/2631-6331/ad335f.

Kiistala, U., 1968. Suction blister device for separation of viable epidermis from dermis. J. Invest. Dermatol. 50, 129–137. https://doi.org/10.1038/jid.1968.15.

Kochhar, J.S., Quek, T.C., Soon, W.J., Choi, J., Zou, S., Kang, L., 2013. Effect of microneedle geometry and supporting substrate on microneedle array penetration into skin. J. Pharmaceut. Sci. 102, 4100–4108. https://doi.org/10.1002/jps.23724.

Kolluru, C., Williams, M., Yeh, J.S., Noel, R.K., Knaack, J., Prausnitz, M.R., 2019. Monitoring drug pharmacokinetics and immunologic biomarkers in dermal interstitial fluid using a microneedle patch. Biomed. Microdevices 21, 14. https://doi.org/10.1007/s10544-019-0363-3.

Kool, J., Reubsaet, L., Wesseldijk, F., Maravilha, R.T., Pinkse, M.W., D'Santos, C.S., Van Hilten, J.J., Zijlstra, F.J., Heck, A.J.R., 2007. Suction blister fluid as potential body fluid for biomarker proteins. Proteomics 7, 3638–3650. https://doi.org/10.1002/pmic.200600938.

Kost, J., Mitragotri, S., Gabbay, R.A., Pishko, M., Langer, R., 2000. Transdermal monitoring of glucose and other analytes using ultrasound. Nat. Med. 6, 347–350. https://doi.org/10.1038/73213.

Krieger, K.J., Bertollo, N., Dangol, M., Sheridan, J.T., Lowery, M.M., O'Cearbhaill, E.D., 2019. Simple and customizable method for fabrication of high-aspect ratio microneedle molds using low-cost 3D printing. Microsyst. Nanoeng. 5, 42. https://doi.org/10.1038/s41378-019-0088-8.

Larrañeta, E., Moore, J., Vicente-Pérez, E.M., González-Vázquez, P., Lutton, R., Woolfson, A.D., Donnelly, R.F., 2014. A proposed model membrane and test method for microneedle insertion studies. Int. J. Pharm. 472, 65–73. https://doi.org/10.1016/j.ijpharm.2014.05.042.

Layani, M., Wang, X., Magdassi, S., 2018. Novel materials for 3D printing by photopolymerization. Adv. Mater. 30, 1706344. https://doi.org/10.1002/adma.201706344.

Li, C.G., Lee, C.Y., Lee, K., Jung, H., 2013. An optimized hollow microneedle for minimally invasive blood extraction. Biomed. Microdevices 15, 17–25. https://doi.org/10.1007/s10544-012-9683-2.

Loh, J.M., Lim, Y.J.L., Tay, J.T., Cheng, H.M., Tey, H.L., Liang, K., 2024. Design and fabrication of customizable microneedles enabled by 3D printing for biomedical applications. Bioact. Mater. 32, 222–241. https://doi.org/10.1016/j.bioactmat.2023.09.022.

Luzuriaga, M.A., Berry, D.R., Reagan, J.C., Smaldone, R.A., Gassensmith, J.J., 2018. Biodegradable 3D printed polymer microneedles for transdermal drug delivery. Lab Chip 18, 1223–1230. https://doi.org/10.1039/C8LC00098K.

Maloney, J.M., Bezzant, J.L., Stephen, R.L., Petelenz, T.J., 1992. Iontophoretic administration of Lidocaine anesthesia in office practice: an appraisal. J. Dermatol. Surg. Oncol. 18, 937–940. https://doi.org/10.1111/j.1524-4725.1992.tb02764.x.

McGrath, M.G., Vucen, S., Vrdoljak, A., Kelly, A., O'Mahony, C., Crean, A.M., Moore, A., 2014. Production of dissolvable microneedles using an atomised spray process: effect of microneedle composition on skin penetration. Eur. J. Pharm. Biopharm. 86, 200–211. https://doi.org/10.1016/j.ejpb.2013.04.023.

Mukerjee, E.V., Collins, S.D., Isseroff, R.R., Smith, R.L., 2004. Microneedle array for transdermal biological fluid extraction and in situ analysis. Sens. Actuators Phys. 114, 267–275. https://doi.org/10.1016/j.sna.2003.11.008.

Nikolov, A., Murad, S., Wasan, D., Wu, P., 2020. How the capillarity and ink-air flow govern the performance of a fountain pen. J. Colloid Interface Sci. 578, 660–667. https://doi.org/10.1016/j.jcis.2020.04.123.

Okereke, M., Keates, S., 2018. Finite element mesh generation. In: Finite Element Applications, Springer Tracts in Mechanical Engineering. Springer International Publishing, Cham, pp. 165–186. https://doi.org/10.1007/978-3-319-67125-3_6.

Raats, P.A.C., 2007. Uptake of water from soils by plant roots. Transport Porous Media 68, 5–28. https://doi.org/10.1007/s11242-006-9055-6.

Rahatuzzaman, M., Mahmud, M., Rahman, S., Hoque, M.E., 2024. Design, fabrication, and characterization of 3D-printed ABS and PLA scaffolds potentially for tissue engineering. Results Eng. 21, 101685. https://doi.org/10.1016/j.rineng.2023.101685.

Rahman, M.M.T., Joyee, E.B., 2022. 3D printed bioinspired hierarchical surface structure with tunable wettability. J. Micro- Nano-Manuf. 10, 041004. https://doi.org/10.1115/1.4064051.

Saddow, S., 2022. Silicon carbide technology for advanced human healthcare applications. Micromachines 13, 346. https://doi.org/10.3390/mi13030346.

Samant, P.P., Niedzwiecki, M.M., Raviele, N., Tran, V., Mena-Lapaix, J., Walker, D.I., Felner, E.I., Jones, D.P., Miller, G.W., Prausnitz, M.R., 2020. Sampling interstitial fluid from human skin using a microneedle patch. Sci. Transl. Med. 12, eaaw0285. https://doi.org/10.1126/scitranslmed.aaw0285.

Samant, P.P., Prausnitz, M.R., 2018. Mechanisms of sampling interstitial fluid from skin using a microneedle patch. Proc. Natl. Acad. Sci. 115, 4583–4588. https://doi.org/10.1073/pnas.1716772115.

Tan, L.J., Zhu, W., Zhou, K., 2020. Recent progress on polymer materials for additive manufacturing. Adv. Funct. Mater. 30, 2003062. https://doi.org/10.1002/adfm.202003062.

Taylor, R.M., Maharjan, D., Moreu, F., Baca, J.T., 2020. Parametric study of 3D printed microneedle (MN) holders for interstitial fluid (ISF) extraction. Microsyst. Technol. 26, 2067–2073. https://doi.org/10.1007/s00542-020-04758-0.

Teymourian, H., Moonla, C., Tehrani, F., Vargas, E., Aghavali, R., Barfidokht, A., Tangkuaram, T., Mercier, P.P., Dassau, E., Wang, J., 2020. Microneedle-based detection of ketone bodies along with glucose and lactate: toward real-time continuous interstitial fluid monitoring of diabetic ketosis and ketoacidosis. Anal. Chem. 92, 2291–2300. https://doi.org/10.1021/acs.analchem.9b05109.

Teymourian, H., Tehrani, F., Mahato, K., Wang, J., 2021. Lab under the skin: Microneedle based wearable devices. Adv. Healthcare Mater. 10, 2002255. https://doi.org/10.1002/adhm.202002255.

Turner, J.G., Lay, E., Jungwirth, U., Varenko, V., Gill, H.S., Estrela, P., Leese, H.S., 2023. 3D-Printed hollow microneedle-lateral flow devices for rapid blood-free detection of c-reactive protein and procalcitonin. Adv. Mater. Technol. 8, 2300259. https://doi.org/10.1002/admt.202300259.

Turner, J.G., White, L.R., Estrela, P., Leese, H.S., 2021. Hydrogel-forming microneedles: current advancements and future trends. Macromol. Biosci. 21, 2000307. https://doi.org/10.1002/mabi.202000307.

Wang, Z., Luan, J., Seth, A., Liu, L., You, M., Gupta, P., Rathi, P., Wang, Y., Cao, S., Jiang, Q., Zhang, X., Gupta, R., Zhou, Q., Morrissey, J.J., Scheller, E.L., Rudra, J.S., Singamaneni, S., 2021. Microneedle patch for the ultrasensitive quantification of protein biomarkers in interstitial fluid. Nat. Biomed. Eng. 5, 64–76. https://doi.org/10.1038/s41551-020-00672-y.

Wu, T., You, X., Chen, Z., 2022. Hollow microneedles on a paper fabricated by standard photolithography for the screening test of prediabetes. Sensors 22, 4253. https://doi.org/10.3390/s22114253.

Yang, J., Yu, R., Li, X., He, Y., Wang, L., Huang, W., Jiao, J., 2021. Silicon carbide whiskers reinforced SiOC ceramics through digital light processing 3D printing technology. Ceram. Int. 47, 18314–18322. https://doi.org/10.1016/j.ceramint.2021.03.152.

Zhang, X., Chen, G., Cai, L., Wang, Y., Sun, L., Zhao, Y., 2021. Bioinspired pagoda-like microneedle patches with strong fixation and hemostasis capabilities. Chem. Eng. J. 414, 128905. https://doi.org/10.1016/j.cej.2021.128905.

Zhang, X., Chen, G., Yu, Y., Sun, L., Zhao, Y., 2020. Bioinspired adhesive and antibacterial microneedles for versatile transdermal drug delivery. Research 2020, 2020/3672120. https://doi.org/10.34133/2020/3672120.